

THREE AXIS ATTITUDE DETERMINATION AND CONTROL SYSTEM FOR A PICO-SATELLITE: DESIGN AND IMPLEMENTATION

Jan Tommy Gravdahl, Egil Eide^a, Amund Skavhaug,
Kjell Magne Fauske, Kristian Svartveit and Fredrik Mietle Indergaard

Department of Engineering Cybernetics and
^aDepartment of Telecommunications
Norwegian University of Science and Technology
N-7491 TRONDHEIM

NORWAY

Revised version

October 7, 2003

Abstract

The design and implementation of the Attitude Determination and Control System (ADCS) for a Norwegian pico-satellite is presented. The satellite, named nCube, is based on the CubeSat concept. This means that its size is restricted to a cube measuring 10 cm on all sides and that its total mass is restricted to 1 kg. Meeting these restrictions represents the main technical challenge of the work. The complete cube includes the payload, ADCS with actuators and sensors, deployable antennas, communication systems, on board data handling (OBDH) and power system. Miniaturization is a key approach in order to meet the tight mass budget. The Determination part of the ADCS is solved by integrating measurements from a three-axis magnetometer with current measurements from the solar panels in a Kalman filter. The solar panels are used as crude sun sensors. The Control part is solved by using a combination of magnetic coils and gravity boom. The control system operates in one of two modes: 1) Detumbling and 2) Stabilization. The control laws are derived using Lyapunov theory, and stringent stability proofs are given. The gravity boom is realized using measurement tape. Simulations of both detumbling, boom deployment and stabilization are presented.

1 Background

On mission from The Norwegian Space Center and Andøya Rocket Range, four Norwegian universities and educational institutes have since 2001 participated in a program to develop a pico satellite known as nCube. A prototype of nCube is shown in Figure 1. The four partners are Narvik University College, Norwegian University of Science and Technology (NTNU), Agricultural

University of Norway, and University of Oslo. The project was split into the subtasks: Mechanical Structure, Power System, Attitude Determination and Control System (ADCS), Payload, Space Communication System (COM), and Ground Segment (GSEG). The ADCS is the responsibility of the Department of Engineering Cybernetics at NTNU, and is the topic of this paper.

The main mission of the satellite is to demonstrate ship traffic surveillance from a LEO satellite using the maritime Automatic Identification System (AIS) recently introduced by the International Maritime Organization (IMO). The AIS system is based on VHF transponders located on board ships. These transponders broadcast the position, speed, heading and other relevant information from the ships at regular time intervals. The main objective of the satellite is to receive, store and retransmit at least one AIS-message from a ship. Another objective of the satellite project is to demonstrate reindeer herd monitoring from space by equipping a reindeer with an AIS transponder during a limited experimental period. In addition, the satellite should maintain communications and digipeater operations using amateur frequencies. A third objective is to demonstrate efficient attitude control using passive gravity gradient stabilization and active magnetic torquers. The arrangement of the antennas and gravity boom is shown in Figure 2. As the system architecture must allow the partners in the project to design and test their systems independently, the basic system architecture does not contain a centralized CPU. Instead, we use a pipelined structure where each subsystem contains their own on board data handlers (OBDH). In Figure 3 a block diagram of the system architecture is shown. The Terminal Node Controller serves as the communications interface to the VHF receiver and the UHF and S-band transmitters. All telecommands are validated by the Telecommand Decoder who forwards the instructions to each sub-



Figure 1: nCube, early prototype

system using the I2C Telecommand Bus. The main subsystems are the AIS receiver, the ADCS and the Power Management Unit. The Data Selector is used to connect the different subsystems to the TNC during transmission down to the ground station. By using this architecture, it is possible to test and verify each subsystem independently during the implementation phase.

The satellite will be placed in a low earth sun synchronous orbit with a perigee of approximately 700 km, and as circular as possible. The inclination will be close to 98° . The launch is scheduled to the second half of 2004 from Dnepr, Ukraine. For further information on the nCube project and detailed description of the satellite the reader is referred to [1] or [2]

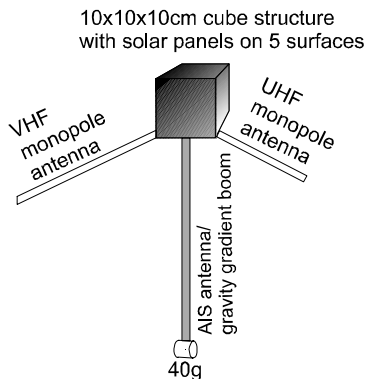


Figure 2: nCube general arrangement including antennas.

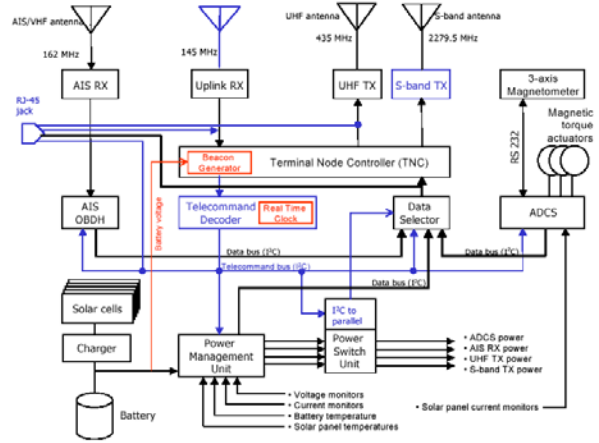


Figure 3: Satellite system architecture

2 Modeling

2.1 Satellite model

2.1.1 Coordinate frames and kinematics

This section describes the definitions of the different reference frames used throughout the paper.

Earth-Centered Inertial (ECI) Reference Frame The origin of this frame is located in the center of the earth. This reference frame will be denoted i , and the earth rotates around its z -axis. The x -axis points towards the vernal equinox, and the y -axis completes a right hand Cartesian coordinate system.

Earth-Centered Earth Fixed (ECEF) Reference Frame The frame shares its origin and z -axis with the ECI frame and is denoted e . The x -axis intersects the earth's surface at latitude 0° and longitude 0° . The ECEF rotates with the earth with a constant angular velocity ω_e , and is therefore not an inertial reference frame.

Orbit Reference Frame The orbit frame origin coincides with the spacecraft center. The origin rotates at an angular velocity ω_o relative to the ECI frame and has its z -axis pointed towards the center of the earth. The x -axis points in the spacecraft's direction of motion tangentially to the orbit. The satellite attitude is described by roll, pitch and yaw which is the rotation around the x -, y -, and z -axis respectively. The orbit reference frame is denoted o .

Body Reference Frame The body frame shares its origin with the orbit frame and is denoted b . The rotation between the orbit frame and the body frame is used to represent the spacecraft's attitude. Its axes are locally defined in the spacecraft, with the origin in the center of gravity or the center of the volume. The nadir side of the spacecraft, intended to point towards the earth, is in the z -axis direction.

The rotation matrix \mathbf{R} from frame a to frame b is denoted \mathbf{R}_a^b . Rotation matrices are members of the special

orthogonal group of order three:

$$\mathbf{R} \in SO(3) = \{\mathbf{R} \mid \mathbf{R} \in \mathbb{R}^{3 \times 3}, \mathbf{R}^T \mathbf{R} = \mathbf{I}, \det \mathbf{R} = 1\} \quad (1)$$

where \mathbf{I} is the 3×3 identity matrix. A transformation of a vector \mathbf{r} from frame a to frame b is written $\mathbf{r}^b = \mathbf{R}_a^b \mathbf{r}^a$. A useful parametrization of the rotation matrix is the angle-axis parametrization, $\mathbf{R}_{\lambda, \theta}$, corresponding to a rotation θ about the λ -axis

$$\mathbf{R}_{\lambda, \theta} = \mathbf{I} + \mathbf{S}(\lambda) \sin \theta + \mathbf{S}^2(\lambda) (1 - \cos \theta). \quad (2)$$

From the orthogonal property in (1), it can be shown [3] that the time derivative of \mathbf{R}_a^b can be written as

$$\dot{\mathbf{R}}_a^b = \mathbf{S}(\boldsymbol{\omega}_{ab}^a) \mathbf{R}_a^b = \mathbf{R}_a^b \mathbf{S}(\boldsymbol{\omega}_{ab}^b) \quad (3)$$

where $\boldsymbol{\omega}_{ab}^b$ is the angular velocity of frame b relative to frame a represented in frame b . The cross product operator is given by

$$\mathbf{S}(\boldsymbol{\omega}) = \boldsymbol{\omega} \times = \begin{pmatrix} 0 & -\omega_z & \omega_y \\ \omega_z & 0 & -\omega_x \\ -\omega_y & \omega_x & 0 \end{pmatrix}, \quad \boldsymbol{\omega} = \begin{pmatrix} \omega_x \\ \omega_y \\ \omega_z \end{pmatrix}.$$

In this paper Euler parameters will be used for representing attitude. The Euler parameter representation of a rotation matrix is given by

$$\eta = \cos(\theta/2), \quad \boldsymbol{\epsilon} = \lambda \sin(\theta/2), \quad (4)$$

where θ and λ are defined in (2). The Euler parameters satisfies

$$\eta^2 + \boldsymbol{\epsilon}^T \boldsymbol{\epsilon} = 1.$$

Using (4), (2) can be written

$$\mathbf{R}_{\eta, \boldsymbol{\epsilon}} = \mathbf{I} + 2\eta \mathbf{S}(\boldsymbol{\epsilon}) + 2\mathbf{S}^2(\boldsymbol{\epsilon}).$$

Generally, the matrix \mathbf{R}_o^b can be written as

$$\mathbf{R}_o^b = (\mathbf{c}_1^b \ \mathbf{c}_2^b \ \mathbf{c}_3^b),$$

where $\mathbf{c}_1^b = (c_{ix}^b \ c_{iy}^b \ c_{iz}^b)^T$ are column vectors. The \mathbf{c}_3^b vector is the projection of the z_o -axis in the body frame. If $\mathbf{c}_3^b = (0 \ 0 \ 1)^T$, the z_b -axis is aligned with the z_o -axis. In this paper c_{iz}^b will be frequently used as a measurement of deviation between the z_b -axis and the z_o -axis.

As shown in [3], the kinematic differential equations can be found from (3) and (4) as

$$\begin{aligned} \dot{\eta} &= -\frac{1}{2} \boldsymbol{\epsilon}^T \boldsymbol{\omega}_{ob}^b \\ \dot{\boldsymbol{\epsilon}} &= \frac{1}{2} (\eta \mathbf{1} + \mathbf{S}(\boldsymbol{\epsilon})) \boldsymbol{\omega}_{ob}^b, \end{aligned} \quad (5)$$

where the angular velocity of the body frame with respect to the orbit frame can be found by

$$\boldsymbol{\omega}_{ob}^b = \boldsymbol{\omega}_{ib}^b - R_o^b \boldsymbol{\omega}_{io}^o = \boldsymbol{\omega}_{ib}^b - \boldsymbol{\omega}_o \mathbf{c}_1^b.$$

2.1.2 Dynamics

Using Euler's moment equation the attitude dynamics of the satellite can be derived as

$$\mathbf{J} \dot{\boldsymbol{\omega}}_{ib}^b + \boldsymbol{\omega}_{ib}^b \times (\mathbf{J} \boldsymbol{\omega}_{ib}^b) = \boldsymbol{\tau}^b, \quad (6)$$

where \mathbf{J} is the inertia matrix of the satellite, $\boldsymbol{\omega}_{ib}^b$ is the angular velocity of the b -frame with respect to the i -frame, decomposed in the b -frame, and

$$\boldsymbol{\tau}^b = \boldsymbol{\tau}_m^b + \boldsymbol{\tau}_g + \boldsymbol{\tau}_a + \boldsymbol{\tau}_s + \boldsymbol{\tau}_m$$

is the torque acting on the satellite. The torque $\boldsymbol{\tau}_m^b$ generated by the magnetotorsquers can be modelled as

$$\boldsymbol{\tau}_m^b = \mathbf{m}^b \times \mathbf{B}^b, \quad (7)$$

where \mathbf{m}^b is the magnetic dipole moment generated by the coils and $\mathbf{B}^b = (B_x \ B_y \ B_z)^T$ is the local geomagnetic field vector. The magnetic dipole moment is given by

$$\mathbf{m}^b = \mathbf{m}_x^b + \mathbf{m}_y^b + \mathbf{m}_z^b = \begin{pmatrix} N_x i_x A_x \\ N_y i_y A_y \\ N_z i_z A_z \end{pmatrix} = \begin{pmatrix} m_x \\ m_y \\ m_z \end{pmatrix},$$

where N_k is the number of windings in the magnetic coil on the axis in the k -direction, i_k is the current in the coil and A_k is the coil area. The disturbance torques $\boldsymbol{\tau}_g$, $\boldsymbol{\tau}_a$, $\boldsymbol{\tau}_s$ and $\boldsymbol{\tau}_m$ will be defined later.

2.2 Environment modeling

2.2.1 The geomagnetic field

For determination of a magnetic vector for comparison with the magnetic vector from the magnetometer, the earth's magnetic field must be known or estimated. The magnetic field is varying strongly over the earth's surface, and a complete table with high resolution is too large to bring on board a satellite's microcontroller. The Earth's magnetic field crudely resembles that of a dipole. The internal geomagnetic field also varies in time, on a time scale of months and longer, in an unpredictable manner. The International Geomagnetic Reference Field, IGRF, is an approximation, near and above the Earth's surface, to that part of the Earth's magnetic field which has its origin in the earth's core. At any one time, the IGRF specifies the numerical coefficients of a truncated spherical harmonic series. The IGRF model is specified every 5 years, for epochs 1900.0, 1905.0 etc. The latest IGRF model specified is thus the IGRF 2000, which is used in the nCube ADCS. Together with an orbit estimator, an estimate of the magnetic field can be made. As the magnetic field revolves with the earth the magnetic field, B , from an IGRF model is in ECEF frame.

2.2.2 Disturbance torques

A satellite is subject to small but persistent disturbance torques. Unless resisted the disturbances will reorient the satellite. The main disturbances are briefly discussed below. The discussion is based on [4] and [5].

Gravity gradient torque The gravity gradient torque τ_g , written in the b -frame as

$$\tau_g^b = 3\omega_0^2 \mathbf{c}_3^b \times (\mathbf{J} \mathbf{c}_3^b), \quad (8)$$

where $\omega_0 \approx (\mu/R_0^3)^{1/2}$, $\mu = GM$ is the Earth's gravitational coefficient and R_0 is the distance to the Earth's center, will affect a non symmetric body in the Earth's gravity field. This effect can be exploited, and will be in the case of nCube, with a gravity boom for passive stabilization.

Aerodynamic torque For low orbit satellites the air density is high enough to influence the satellite's attitude dynamics. The aerodynamic torque can be written as

$$\tau_a = \frac{1}{2} \rho V^2 C_d A (\mathbf{u}_v \times \mathbf{s}_{cp}),$$

where ρ is the atmospheric density, V is velocity, C_d is the drag coefficient, \mathbf{u}_v is the unit vector in the velocity direction, A is area perpendicular to \mathbf{u}_v and \mathbf{s}_{cp} is the vector distance from center of mass to center of pressure.

Solar radiation torque Radiation and particles from the Sun affect the satellite. For low orbit satellite's the effect is negligible compared with other disturbances. An expression for the worst-case disturbance is

$$\tau_s = F (c_{ps} - c_g), \quad F = \frac{F_s}{c} A_s (1 + q) \cos i,$$

where $F_s = 1367 \text{W/m}^2$ is the solar constant, c is the speed of light, A_s is the surface area, c_{ps} is the center of solar pressure, c_g is the center of gravity, $q \in [0, 1]$ is the reflectance factor, and i is the angle of incidence of the Sun.

Magnetic field The electronics in the satellite may create an unwanted residual magnetic dipole. This field will interact with the Earth's geomagnetic field. The resulting torque can be written as

$$\tau_m = DB,$$

where D is the residual dipole of the satellite and B is the Earth's magnetic field.

Also, disturbances may have their source in the external geomagnetic field. This field varies on a faster time-scale than the internal geomagnetic field. Moreover, the external field may vary in an unpredictable manner.

Boom distortion The gravity gradient boom is modelled as an ideal rigid body. In the real world temperature changes and environment disturbances will distort the boom, resulting in oscillations that may disturb the satellite. It is important to determine the resonance frequencies and design the control system in a way that does not excite structural resonances [6]. Gravity boom construction and design for nCube is addressed in [7], and will be presented in Section 5.1.2.

In Table 1, [8] has calculated the worst case numerical values for nCube.

Disturbance	Magnitude [Nm]
Gravity gradient	$1.0382 \cdot 10^{-7}$
Aerodynamic drag	$3.65 \cdot 10^{-9}$
Solar radiation	$1.5371 \cdot 10^{-8}$
Internal field	$1 \cdot 10^{-6}$

Table 1: Disturbance torques for Ncube

3 Controller design

3.1 Energy considerations

An important tool in control theory is the use of energy-based controllers based on Lyapunov designs and passivity [3]. In this section expressions for the satellite's energy is presented, and a suitable Lyapunov function candidate and its derivative is found.

The energy of the satellite can be divided into kinetic and potential energy. The kinetic energy is mainly due to rotation in the inertial and orbit frame, while the most important source to potential energy is the gravity gradient and gyro effects due to revolution about the Earth. The expressions for kinetic and potential energy is based on [9], [10] and [11]. From a control perspective the rotation of the body frame with respect to the orbit frame is most interesting. Assuming a near circular orbit, and therefore a constant orbital rate ω_o , the kinetic energy can be written

$$E_{kin} = \frac{1}{2} (\boldsymbol{\omega}_{ob}^b)^T \mathbf{J} \boldsymbol{\omega}_{ob}^b. \quad (9)$$

The potential energy due to the gravity gradient is

$$E_{gg} = \frac{3}{2} (\omega_o^2 (\mathbf{c}_3^b)^T \mathbf{J} \mathbf{c}_3^b - I_z), \quad (10)$$

and the potential energy due to the revolution of the satellite about the Earth is given by

$$E_{gyro} = \frac{1}{2} \omega_o^2 (I_x - (\mathbf{c}_1^b)^T \mathbf{J} \mathbf{c}_1^b). \quad (11)$$

Defining

$$\mathbf{x} = (\boldsymbol{\omega}_{ob}^b \ c_{21} \ c_{31} \ c_{13} \ c_{23})^T \in \mathbb{R}^7,$$

and using (9), (10) and (11), it can be seen that the energy function V defined by

$$\begin{aligned} V(\mathbf{x}) &= E_{kin} + E_{gg} + E_{gyro} = \frac{1}{2} (\boldsymbol{\omega}_{ob}^b)^T \mathbf{J} \boldsymbol{\omega}_{ob}^b \\ &+ \frac{3}{2} \omega_o^2 ((I_x - I_z) c_{13}^2 + (I_y - I_z) c_{23}^2) \\ &+ \frac{1}{2} \omega_o^2 ((I_x - I_y) c_{21}^2 + (I_x - I_z) c_{31}^2) \end{aligned} \quad (12)$$

satisfies $V(\mathbf{0}) = 0$. The simplifications in the last two terms of (12) follows from the fact that \mathbf{R}_o^b is orthogonal. In order to ensure that V is positive definite, that is $V > 0 \forall \mathbf{x} \neq \mathbf{0}$, we require that

$$I_x > I_y > I_z.$$

For use in the stability analysis of the controller we need an expression for the time derivative of (12)

$$\dot{V} = (\boldsymbol{\omega}_{ob}^b)^T \mathbf{J} \dot{\boldsymbol{\omega}}_{ob}^b + 3\omega_o^2 (\mathbf{c}_3^b)^T \mathbf{J} \dot{\mathbf{c}}_3^b - \omega_o^2 (\mathbf{c}_1^b)^T \mathbf{J} \dot{\mathbf{c}}_1^b. \quad (13)$$

It follows from (6) and (8) that the satellite dynamics, considering the gravity gradient and magnetic coil torques only, can be written as

$$\mathbf{J} \dot{\boldsymbol{\omega}}_{ib}^b + \boldsymbol{\omega}_{ib}^b \times (\mathbf{J} \boldsymbol{\omega}_{ib}^b) = 3\omega_o^2 \mathbf{c}_3^b \times (\mathbf{J} \mathbf{c}_3^b) + \boldsymbol{\tau}_m^b. \quad (14)$$

Using (14) and the relations $\boldsymbol{\omega}_{ib} = \boldsymbol{\omega}_{ob} + \omega_o \mathbf{c}_1^b$, $(\boldsymbol{\omega}_{ob}^b)^T \mathbf{S}(\boldsymbol{\omega}_{ob}^b) = \mathbf{0}$ and

$$\dot{\mathbf{c}}_i^b = \mathbf{S}(\mathbf{c}_i^b) \boldsymbol{\omega}_{ob}^b, \quad (15)$$

(13) is written

$$\begin{aligned} \dot{V} &= (\boldsymbol{\omega}_{ob}^b)^T \left(3\omega_o^2 \mathbf{S}(\mathbf{c}_3^b) \mathbf{J} \mathbf{c}_3^b + \boldsymbol{\tau}_m^b - \omega_o \mathbf{J} \mathbf{S}(\mathbf{c}_1^b) \boldsymbol{\omega}_{ob}^b \right. \\ &\quad \left. - \omega_o \mathbf{S}(\mathbf{c}_1^b) \mathbf{J} \boldsymbol{\omega}_{ob}^b - \omega_o^2 \mathbf{S}(\mathbf{c}_1^b) \mathbf{J} \mathbf{c}_1^b \right) \\ &\quad + 3\omega_o^2 (\mathbf{c}_3^b)^T \mathbf{J} \mathbf{S}(\mathbf{c}_3^b) \boldsymbol{\omega}_{ob}^b - \omega_o^2 (\mathbf{c}_1^b)^T \mathbf{J} \mathbf{S}(\mathbf{c}_1^b) \boldsymbol{\omega}_{ob}^b. \end{aligned} \quad (16)$$

Since $\mathbf{S}^T(\mathbf{x}) = -\mathbf{S}(\mathbf{x})$, (16) is reduced to

$$\dot{V} = (\boldsymbol{\omega}_{ob}^b)^T \boldsymbol{\tau}_m^b. \quad (17)$$

Remark 1 *The equilibrium*

$$\mathbf{x} = (\boldsymbol{\omega}_{ob}^b \ c_{21} \ c_{31} \ c_{13} \ c_{23})^T = \mathbf{0},$$

corresponds to four equilibria

$$(\boldsymbol{\omega}_{ob}^b \ \mathbf{c}_3^b \ \mathbf{c}_1^b)^T = (\mathbf{0} \ \pm \mathbf{c}_3^o \ \pm \mathbf{c}_1^o)^T$$

for the satellite.

3.2 Detumbling

When the satellite is released from the launcher it will have an initial angular velocity. Before a boom can be deployed the angular velocity must be reduced and the body frame must be aligned with the orbit frame. The detumbling phase can be divided into rate detumbling and angle detumbling. In the rate detumbling mode the kinetic energy of the satellite must be dumped and the angular velocity of the body frame with respect to the inertial frame reduced. High angular velocities make it difficult to estimate the satellite's orientation. The requirements of the rate detumbling mode is that the angular velocities must be reduced to a value below $\boldsymbol{\omega}_{ob}^b < (5 \cdot 10^{-3} \ 5 \cdot 10^{-3} \ 5 \cdot 10^{-3})^T$. The only sensor available in this mode will be the magnetometer. After the rate detumbling phase the satellite may have an arbitrary attitude. Before the boom can be deployed we must ensure that the body z_b -axis is aligned with the orbit z_o -axis. If the boom is deployed in the opposite direction it may be difficult to

turn the satellite. For boom deployment we require that the deviation between the z_b and z_o axes is less than 30° .

The objective of the rate detumbling controller is to dissipate the kinetic energy of the satellite. A controller which uses only rate measurements from the magnetometers is suggested below. The controller is proposed in [11], [6] and [10].

Proposition 2 *The control law*

$$\mathbf{m}^b = -k \dot{\mathbf{B}}^b - \mathbf{m}_c, \quad (18)$$

where $\mathbf{m}_c = (0 \ 0 \ m_c)^T$ will dissipate the kinetic energy of the satellite and align it with the local geomagnetic field.

To prove that the energy is dissipated, Lyapunov theory will be used. The proof is based on [11] and [6].

By combining (7) and (18), the control torque $\boldsymbol{\tau}_m^b$ is given by

$$\boldsymbol{\tau}_m^b = \mathbf{m}^b \times \mathbf{B}^b = (-k \dot{\mathbf{B}}^b - \mathbf{m}_c) \times \mathbf{B}^b. \quad (19)$$

We note that the magnetic field vector \mathbf{B}^b can be written as $\mathbf{B}^b = \mathbf{R}_i^b \mathbf{B}^i$, and consequently

$$\dot{\mathbf{B}}^b = \dot{\mathbf{R}}_i^b \mathbf{B}^i + \mathbf{R}_i^b \dot{\mathbf{B}}^i = \mathbf{B}^b \times \boldsymbol{\omega}_{ib}^b + \mathbf{R}_i^b \dot{\mathbf{B}}^i. \quad (20)$$

Near the North and South Poles, \mathbf{B}^b is approximately constant. Equation (21) can therefore be approximated as

$$\dot{\mathbf{B}}^b \approx \mathbf{B}^b \times \boldsymbol{\omega}_{ib}^b \quad (21)$$

This assumption is valid only in the polar regions. When the boom is stowed, the gravity gradient will be very small and can be neglected, however the constant term in (18) will contribute to the potential energy. Thus, the sum of kinetic T and potential energy U can be written as

$$V = T + U = \frac{1}{2} (\boldsymbol{\omega}_{ib}^b)^T \mathbf{J} \boldsymbol{\omega}_{ib}^b + |\mathbf{m}_c| |\mathbf{B}^b| + \mathbf{m}_c^T \mathbf{B}^b. \quad (22)$$

Assuming a constant magnitude of the geomagnetic field in the polar regions, the time derivative of (22) is

$$\dot{V} = (\boldsymbol{\omega}_{ib}^b)^T \boldsymbol{\tau}_m^b + \mathbf{m}_c^T \dot{\mathbf{B}}^b,$$

and using (19) and (21) it follows that

$$\begin{aligned} \dot{V} &= (\boldsymbol{\omega}_{ib}^b)^T \left((-k \dot{\mathbf{B}}^b - \mathbf{m}_c) \times \mathbf{B}^b \right) + \mathbf{m}_c^T \dot{\mathbf{B}}^b \\ &= -k (\dot{\mathbf{B}}^b)^T \dot{\mathbf{B}}^b \end{aligned}$$

which is negative semidefinite. We conclude that energy is dissipated and the angular velocities are reduced.

Remark 3 *The z_b -axis will tend to point along \mathbf{B}^i . This is not shown in the analysis above, but a proof can be found in [10] or [6]. Near the poles \mathbf{B}^i points vertically upwards, meaning that in the polar regions the deviation of the z_b -axis from nadir will be relatively small. This can be utilized for boom deployment.*

3.3 Stabilization

We will here use the same control law as in [11]. Asymptotic stability of Wisniewski's controller was proven by assuming Earth's magnetic field to be periodic and then using the Krasovskii-LaSalle theorem [12]. As discussed in Section 2.2.2, the magnetic field may vary with time in an unpredictable manner. Our contribution to previous work is to use Matrosov's theorem [13] as stated in [14] in order to prove global uniform asymptotic stability (GUAS) of the equilibrium without assuming periodicity of the geomagnetic field $\mathbf{B}^b(t)$.

Proposition 4 *The control law*

$$\mathbf{m}^b = \mathbf{H}\boldsymbol{\omega}_{ob}^b \times \mathbf{B}^b, \quad (23)$$

makes the origin, $\mathbf{x} = \mathbf{0}$ of the system (14), (15) GUAS.

Proof. Define

$$\begin{aligned} V_1 = V &= \frac{1}{2} (\boldsymbol{\omega}_{ob}^b)^T \mathbf{J} \boldsymbol{\omega}_{ob}^b + \frac{3}{2} (\boldsymbol{\omega}_o^2 (\mathbf{c}_3^b)^T \mathbf{J} \mathbf{c}_3^b - I_z) \\ &+ \frac{1}{2} \omega_o^2 (I_x - (\mathbf{c}_1^b)^T \mathbf{J} \mathbf{c}_1^b), \end{aligned} \quad (24)$$

where the LFK in equation (12) has been used. Using (23) and calculating the time derivative of (24) along the trajectories of (14), (15) results in

$$\begin{aligned} \dot{V}_1 &= (\boldsymbol{\omega}_{ob}^b)^T (\mathbf{H}\boldsymbol{\omega}_{ob}^b \times \mathbf{B}^b \times \mathbf{B}^b) \\ &= -(\boldsymbol{\omega}_{ob}^b)^T \mathbf{S}^T (\mathbf{B}^b) \mathbf{S} (\mathbf{B}^b) \mathbf{H}\boldsymbol{\omega}_{ob}^b = Y_1 \leq 0, \end{aligned} \quad (25)$$

as shown in equations (13) to (17). The Lyapunov function candidate (24) is positive definite and its time derivative (25) is negative semidefinite. It follows that the origin is UGS, and Assumption 1 of Theorem 1 in [14] is satisfied. Moreover, Assumption 2 is satisfied for $i = 1$. Define the auxiliary function V_2 .

$$V_2 = -\mathbf{c}_3^T \mathbf{J}^T \mathbf{S}^T (\mathbf{c}_3) \mathbf{J} \boldsymbol{\omega}_{ob}^b,$$

where the b superscript on $\mathbf{c}_{1,2}^b$ has been dropped for notational convenience. Now,

$$\begin{aligned} \dot{V}_2 &= -\dot{\mathbf{c}}_3^T \mathbf{J}^T \mathbf{S}^T (\mathbf{c}_3) \mathbf{J} \boldsymbol{\omega}_{ob}^b - \mathbf{c}_3^T \mathbf{J}^T \mathbf{S}^T (\dot{\mathbf{c}}_3) \mathbf{J} \boldsymbol{\omega}_{ob}^b \\ &- \mathbf{c}_3^T \mathbf{J}^T \mathbf{S}^T (\mathbf{c}_3) \mathbf{J} \dot{\boldsymbol{\omega}}_{ob}^b. \end{aligned}$$

As the system is stable, it follows that the states are bounded. Using the same notation as in [14], we let the number ν denote a generic bound on continuous functions, and \dot{V}_2 can be upper bounded as

$$\dot{V}_2 \leq -\mathbf{c}_3^T \mathbf{J}^T \mathbf{S}^T (\mathbf{c}_3) \mathbf{J} \dot{\boldsymbol{\omega}}_{ob}^b + \nu_1 |\boldsymbol{\omega}_{ob}^b|,$$

and using (14) further bounded as

$$\begin{aligned} \dot{V}_2 &\leq -\mathbf{c}_3^T \mathbf{J}^T \mathbf{S}^T (\mathbf{c}_3) (3\omega_o^2 \mathbf{S} (\mathbf{c}_3) \mathbf{J} \mathbf{c}_3 \\ &- \omega_o^2 \mathbf{S} (\mathbf{c}_1) \mathbf{J} \mathbf{c}_1) + \nu_2 |\boldsymbol{\omega}_{ob}^b| \\ &\leq -2\omega_o^2 \mathbf{c}_3^T \mathbf{J}^T \mathbf{S}^T (\mathbf{c}_3) \mathbf{S} (\mathbf{c}_3) \mathbf{J} \mathbf{c}_3 + \nu_2 |\boldsymbol{\omega}_{ob}^b|, \end{aligned}$$

where it has been used that $\mathbf{c}_{1,2}$ are unit vectors. Now, we see that

$$Y_1 \equiv 0$$

\Downarrow

$$\dot{V}_2 \leq -2\omega_o^2 \mathbf{c}_3^T \mathbf{J}^T \mathbf{S}^T (\mathbf{c}_3) \mathbf{S} (\mathbf{c}_3) \mathbf{J} \mathbf{c}_3 = Y_2 \leq 0,$$

and Assumption 2 and 3 are satisfied for $i = 2$. Defining the auxiliary function V_3 as

$$V_3 = \mathbf{c}_1^T \mathbf{J}^T \mathbf{S}^T (\mathbf{c}_1) \mathbf{J} \boldsymbol{\omega}_{ob}^b,$$

and calculating its time derivative in the same manner as for \dot{V}_2 results in

$$\begin{aligned} \dot{V}_3 &= \dot{\mathbf{c}}_1^T \mathbf{J}^T \mathbf{S}^T (\mathbf{c}_1) \mathbf{J} \boldsymbol{\omega}_{ob}^b + \mathbf{c}_1^T \mathbf{J}^T \mathbf{S}^T (\dot{\mathbf{c}}_1) \mathbf{J} \boldsymbol{\omega}_{ob}^b \\ &+ \mathbf{c}_1^T \mathbf{J}^T \mathbf{S}^T (\mathbf{c}_1) \mathbf{J} \dot{\boldsymbol{\omega}}_{ob}^b \\ &\leq \mathbf{c}_1^T \mathbf{J}^T \mathbf{S}^T (\mathbf{c}_1) \mathbf{J} \dot{\boldsymbol{\omega}}_{ob}^b + \nu_3 |\boldsymbol{\omega}_{ob}^b| \\ &\leq \mathbf{c}_1^T \mathbf{J}^T \mathbf{S}^T (\mathbf{c}_1) (3\omega_o^2 \mathbf{S} (\mathbf{c}_3) \mathbf{J} \mathbf{c}_3 \\ &- \omega_o^2 \mathbf{S} (\mathbf{c}_1) \mathbf{J} \mathbf{c}_1) + \nu_4 |\boldsymbol{\omega}_{ob}^b| \\ &\leq -\omega_o^2 \mathbf{c}_1^T \mathbf{J}^T \mathbf{S}^T (\mathbf{c}_1) \mathbf{S} (\mathbf{c}_1) \mathbf{J} \mathbf{c}_1 \\ &+ \nu_4 |\boldsymbol{\omega}_{ob}^b| + \nu_5 |\mathbf{c}_3|, \end{aligned}$$

where the fact that $\boldsymbol{\omega}_{ob}^b$ and \mathbf{c}_3 are bounded has been used. Now

$$Y_1 \equiv Y_2 \equiv 0$$

\Downarrow

$$\dot{V}_3 \leq -\omega_o^2 \mathbf{c}_1^T \mathbf{J}^T \mathbf{S}^T (\mathbf{c}_1) \mathbf{S} (\mathbf{c}_1) \mathbf{J} \mathbf{c}_1 = Y_3 \leq 0,$$

and Assumption 2 and 3 are satisfied for $i = 3$. Finally

$$Y_i = 0, \quad i = \{1, 2, 3\} \implies \mathbf{x} = \mathbf{0},$$

and Assumption 4 of [14] is satisfied and the result follows. ■

Remark 5 *In the two equilibria $(\boldsymbol{\omega}_{ob}^b \mathbf{c}_3^b \mathbf{c}_1^b) = (\mathbf{0} - \mathbf{c}_3^o \pm \mathbf{c}_1^o)$ the gravity boom is pointing in the wrong direction.*

Depending on the initial conditions, the angular velocity feedback controller in (23) drives the system to any one of the four possible equilibria. It is desirable to have a control procedure that makes the satellite tend to the desired orientation from all initial conditions. An interesting question in this context is how much potential energy is necessary to make the boom axis cross the horizontal plane. From the discussions in Section 3.1 it follows that the minimum energy necessary is $E_{gg}^y = \frac{3}{2} \omega_o^2 (I_y - I_z)$, while the maximum energy needed is $E_{gg}^x + E_{gyro}^z = 2\omega_o^2 (I_x - I_z)$. If the total energy $V < E_{gg}^y$ the boom axis can't cross the horizontal plane. This means that if initially $\mathbf{c}_{3z}^b > 0$ and the controller (23) is used, the satellite will converge to $(\boldsymbol{\omega}_{ob}^b \mathbf{c}_3^b \mathbf{c}_1^b) = (\mathbf{0} \mathbf{c}_3^o \pm \mathbf{c}_1^o)$. If the controller is used only when $\mathbf{c}_{3z}^b > 0$, the total energy will be dissipated. Turning off the controller when $\mathbf{c}_{3z}^b \leq 0$ keeps the energy level constant. If the energy level is large enough, the boom axis will again cross the horizontal plane. Turning on the controller again will further dissipate the energy until the satellite converges to the desired equilibrium.

3.4 Inverted boom recovery

If the attitude control system temporarily fails, or the boom is released in the wrong direction, the boom axis may end up pointing below the horizontal plane. The procedures described in the previous sections will then fail, since $c_{3z}^b < 0$. A solution to this is to apply a destabilizing controller that eventually makes the boom axis to appear above the horizontal plane. The satellite should be rotated in a way that requires a minimum amount of energy. If the boom axis is below the horizon, the destabilizing controller

$$\mathbf{m}^b = k_{br} \mathbf{c}_1^b \times \mathbf{B}^b, \quad (26)$$

where $k_{br} > 0$ is a constant, is a minimum effort controller that turns the boom axis above the horizontal plane. The idea of the controller (26) is to generate a minimal effort torque in the direction that requires a minimum of potential energy. A minimal effort torque is achieved if the control torque is perpendicular to the local geomagnetic field. As the x -component of the local geomagnetic field is much smaller than the y and z components, the geomagnetic field vector \mathbf{B}^o is approximately perpendicular to the \mathbf{x}^o , or \mathbf{c}_1^o vector. This is valid also in the body frame, hence the generated torque is

$$\begin{aligned} \boldsymbol{\tau}_m^b &= k \mathbf{B}^b \times (\mathbf{B}^b \times \mathbf{c}_1^b) \\ &= k \left(((\mathbf{B}^b)^T \mathbf{c}_1^b) \mathbf{B}^b - ((\mathbf{B}^b)^T \mathbf{B}^b) \mathbf{c}_1^b \right) \\ &\approx -k \left((\mathbf{B}^b)^T \mathbf{B}^b \right) \mathbf{c}_1^b, \end{aligned}$$

where we have used that the scalar product of two perpendicular vectors is zero. Since \mathbf{c}_1^b is approximately perpendicular to \mathbf{B}^b , (26) is a minimum effort controller.

4 Attitude determination

The determination part of the ADCS for nCube will consist of a magnetometer and sun sensor. The sun sensor will be implemented taking advantage of the relation between current output from the solar panels and the direction towards the sun. The current I_i from a solar panel i is

$$I_i = I_{\max} \sin \alpha_i, \quad (27)$$

where I_{\max} is the current output at angle of attack $\alpha_i = \frac{\pi}{2}$. In [15] it is shown that a sun vector \mathbf{v}_S^b in b -coordinates can be found as

$$\mathbf{v}_S^b = (k_x I_1 \ k_y I_2 \ k_z I_3)^T, \quad (28)$$

where k_x, k_y and k_z equals ± 1 depending on whether the solar cells on the positive or negative side of the satellite are delivering current, and hence points towards the sun. In the computations I_{\max} is eliminated, and this is crucial as I_{\max} depends directly on the load resistance, which is highly variable, and depends on which subsystems are being used, and on whether the batteries are being recharged or not. The accuracy of the coarse sun sensor is deteriorated heavily by the reflection of the suns energy from the

earth. Only half the earth is illuminated by the sun, and only parts, if any, of this half is visible from the satellite. In [16], a method for predicting the influence of the energy reflected from earth on a coarse sun sensor is presented. This method is planned to be used in the nCube project.

A magnetometer can only be used in orbit close to earth where the magnetic field is strong and well modelled. As the nCube is to orbit at approximately 700km, a Low Earth Orbit, LEO, this is feasible. The magnetometer consists of three orthogonal sensor elements which measure the earths magnetic field in three axes in the sensor frame. If the magnetometer is aligned with the satellites axes, or the rotation between the body and sensor frame is known, the magnetic field in the body frame is obtained. This measurement is compared in the Kalman filter, to a model of the earths magnetic field which gives the magnetic field in orbit coordinates. The most used model is the IGRF, presented in Section 2.2.1.

A discrete Extended Kalman Filter (EKF) is used for estimating the attitude. Details on Kalman filter design can be found in e.g. [17]. The state vector

$$x = (\epsilon \ \eta \ \omega_{ib}^b)^T,$$

where ϵ and η are the Euler parameter representation of attitude given in (15) and (5). The magnetometer measurement \mathbf{B}_{meas}^b is normalized as it is only the direction, and not the length of the vector that gives attitude information. In the remainder of this Section, all magnetic field vectors, both from the magnetometer, and from the IGRF model, are assumed normalized. The measurement is related to the earth's magnetic field \mathbf{B}^e through

$$\mathbf{B}_{meas}^b = \mathbf{R}_e^b \mathbf{B}^e$$

This equation can also give the estimated measurement when \mathbf{R}_e^b is based on the estimate of the quaternion $\mathbf{q} = (\epsilon \ \eta)^T$, and \mathbf{B}^e is the IGRF model of the earth's magnetic field:

$$\begin{aligned} \widehat{\mathbf{B}}^b &= \widehat{\mathbf{R}}_e^b \mathbf{B}_{IGRF}^e \\ \widehat{\mathbf{B}}^b &= \mathbf{R}_e^b(\widehat{\mathbf{q}}) \mathbf{B}_{IGRF}^e \end{aligned}$$

Where $(\widehat{\cdot})$ denotes an estimate. The updating of the state vector estimate is divided into a quaternion part and an angular velocity part. \mathbf{K}_q and \mathbf{K}_ω is used to denote the two corresponding parts of the Kalman filter gain. We will use the innovation,

$$\boldsymbol{\nu} = \mathbf{B}_{meas}^b \times \mathbf{R}_e^b(\widehat{\mathbf{q}}) \mathbf{B}_{IGRF}^e$$

suggested by [18]. The corresponding update of the quaternion is suggested as

$$\widehat{\mathbf{q}} = \widehat{\mathbf{q}}^- \otimes \left(\frac{\Delta \mathbf{q}_{ud}}{\sqrt{1 - |\Delta \mathbf{q}_{ud}|^2}} \right),$$

where $\Delta \mathbf{q}_{ud} = \mathbf{K}_q \boldsymbol{\nu}$. The angular velocity is updated with the same innovation, but with normal Kalman filter update

$$\widehat{\omega}_{ib}^b = \widehat{\omega}_{ib}^{b-} + \mathbf{K}_\omega \boldsymbol{\nu}.$$

The nonlinear measurement matrix \mathbf{H} must be linearized around the estimate to calculate the Kalman filter gain. The linearization yields, according to [19]

$$\mathbf{H} = (2\mathbf{S}(\mathbf{B}^b) \mathbf{0})$$

This matrix has only rank two which implies that no information about rotation around the magnetic field vector is available. The system is not observable with only the magnetometer measurement, but as the Kalman filter utilizes historical information an estimate can still be computed.

In principle the sun sensor measurement, and the magnetometer measurement, can be treated similar as they are both reference sensors providing a vector to be compared with a known vector. The Kalman filter is ideal to fuse different measurements as they are modelled with different covariances, and thus will be weighted different in the estimate update through the Kalman filter gain. The measurement matrix including the sun sensor measurement will be

$$\mathbf{H} = \begin{pmatrix} 2\mathbf{S}(\mathbf{B}^b) & \mathbf{0} \\ 2\mathbf{S}(\mathbf{v}_S^b) & \mathbf{0} \end{pmatrix}$$

where \mathbf{v}_S^b is the sun vector in body coordinates as defined in equation (28).

5 ADCS Implementation

5.1 Choice of components

5.1.1 Sensors

The digital magnetometer HMR 2300 from Honeywell will be used. It is mounted on a $7.49 \times 3.05 \text{ cm}$ circuit board weighing 28 g . This board gives the magnetometer a digital interface with a 9600 baud serial RS232 communication through a nine pin connector. There are no offset possibilities, but as long as the total magnetic field is within the magnetometers range, the offset could be done in the satellites on board microcontroller.

The University of Oslo together with the Institute for Energy Technology will produce all the solar cells needed. These cells are single junction silicone cells with an efficiency of 18%. The advantage with custom made cells is that the surface of the satellite can be completely covered.

5.1.2 Actuators

For actuation of the satellite, magnetic torque coils will be used. The coils are produced at the motor winding lab at NTNU. The coils outer dimensions are $66 \times 66 \text{ mm}$, the inner dimensions are $58 \times 58 \text{ mm}$, and the thickness is 3 mm , as shown in Figure 4. The number of windings is $N = 140$.

The gravity boom will be constructed from measuring tape. It has a length of 1.5 m , thickness 1 mm , width 13 mm and has a tip-mass of 40 g . The boom is constructed the following way: One end of measuring tape



Figure 4: Photo of one of the torque coils

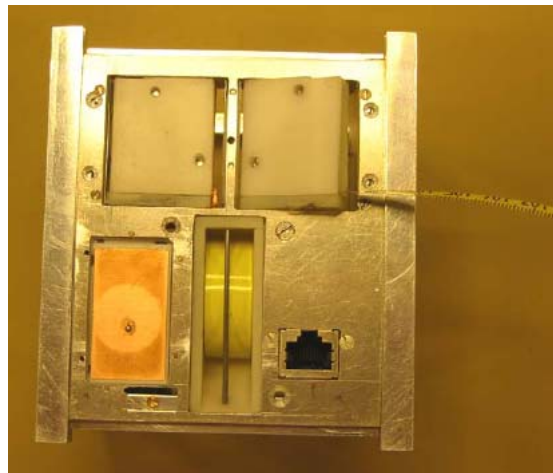


Figure 5: Photo of the nadir surface of Ncube. The gravity boom is coiled up and restrained inside its box.

is attached to a metal cylinder (with a screw). The measuring tape will act as the boom rod, and the metal cylinder as the tip-mass when deployed. To store the boom before deployment the loose end of the measuring tape is attached to the containment box and the tape is then coiled around the cylinder. When the tape is coiled all the way up it is constrained to the box with fishing line which is tightened around the box. The fishing line is knotted to one side of the box and screwed to another, to make it possible to tighten the line sufficiently. Two Nichrome wires are coiled around the fishing line and connected to the batteries. The boom deployment is done by applying a voltage of 3.6 V to the Nichrome wires which will make them melt the fishing line (two wires are used for redundancy) and thus release boom. Further details regarding the gravity boom construction can be found in [7].

5.1.3 Computer system

It soon became clear that the requirements for the computer system were difficult to fulfill with just one microcontroller. It should use very little power, be physically small and at the same time be able to handle heavy floating-point calculations for the Kalman filter and equation sets. Since most of the simulations and theoretical

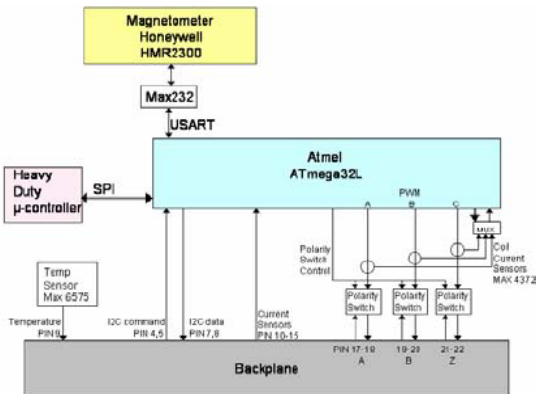


Figure 6: Attitude control system block diagram

work were done with Matlab and Simulink, we wanted to be able to use Real-Time Workshop for code-generation. This to avoid translation errors, and to facilitate rapid changes to the math followed by experiments. This pointed to the use of a modern RISC 32bit CPU supported either by VxWorks or Linux. On the other hand, we had to be able to do low-level hardware access with highly predictable timing properties, and maybe more important: The practical issues around the student groups participating in the implementation made it clear that we had to choose both SW tools and a HW platform which at least some of them knew very well. Therefore a solution with two loosely coupled CPUs with very different characteristics were chosen. See Figure 6. For all the tasks, except those with heavy calculations, an Atmel AVR Mega 128 were used. This way we could finish the hardware related part immediately, only by using tools readily available, and in addition re-use many of the subroutines used in other parts of the system. For this AVR-part we built a small PCB with all the necessary electronics and connections for the sensor and actuators. The communication with the “calculation CPU” is done with a simple SPI interface. Since modern 32 bit CPUs require advanced equipment just to solder, and introduces a number of challenges for the non-professional when flash and RAM shall be connected, we searched for a pre-built daughter card that only included CPU, RAM and flash memory with the right characteristics regarding power consumption, connectivity, size, OS support etc. Later it became clear that this division was indeed very useful, when the small ARM-based CPU-card from Advantech we had chosen would not be available despite samples already given to industrial partners who recommended it to us. This simple and very loosely coupled interface between low-level control and calculations then made it possible for us to look for another 32-bit CPU daughter-card without stopping the other tests, and furthermore, this division makes it possible for us to try out the Matlab generated code with an ordinary PC equipped with a simple SPI-interface-card for the calculations.

5.2 Testing

5.2.1 Gravity boom

The release mechanism for the gravity boom has been tested in a vacuum chamber and a cold environment with satisfying results. The testing of the gravity boom was accepted by ESA for participation in the 6th ESA student parabolic flight campaign during 16-25 July 2003. The purpose of the campaigns are to stimulate space research among students all over Europe and it is part of ESAs outreach program. 120 students are selected (30 teams of four) for each campaign. The parabolic flight is performed by Novespace and the aircraft used is an Airbus 300. Two flights per experiment was performed, where each flight consisted of 30 parabolas. The parabolic flight and accommodation were both financed by ESA. The main objective of the experiment was to test the deployment system repeatedly under a controlled micro-g environment, and observe the effects of a deployment on the satellite. The experiment was documented visually by a camera, and the satellite was also equipped with a 3-axis accelerometer and gyros whose raw data was stored in a laptop. In order to fulfill the safety requirements during the flights, the satellite had to be restrained by ropes, and this unfortunately decreased the possible free-floating time. However, several successful boom deployments were conducted. The tests can be found in [7].

5.2.2 Solar vector from solar panel currents

The relation between solar panel current and angle of attack in equation (27) is experimentally verified in [15].

6 Simulations

Now the controllers for detumbling, stabilization and inverted boom recovery will be simulated. The parameters of the model used in the simulations are: Body size $10 \times 10 \times 10$ cm, boom length: 1.5 m, moments of inertia, boom stowed: $I_x = 0.0621 \text{ kgm}^2$, $I_y = 0.0606 \text{ kgm}^2$, $I_z = 0.0031 \text{ kgm}^2$, moments of inertia, boom deployed: $I_x = 0.3210 \text{ kgm}^2$, $I_y = 0.1806 \text{ kgm}^2$, $I_z = 0.0031 \text{ kgm}^2$, maximum magnetic moment from the coils: 0.1 Am^2 .

6.1 Detumbling mode

The detumbling mode controller (18) was simulated with initial values: $\omega_{ib}^b = (0.1 \ 0.1 \ 0.09)^T \text{ rad/s}$ and controller parameters: $k = 10^4$ and $m_c = -0.01 \text{ Am}^2$. In Figure 7 it is shown that the angular velocities are quickly reduced and the z_b -axis aligns itself with the geomagnetic field vector. Average power consumption is $\bar{P} = 5 \text{ mW}$, while the total energy used is $E = 123 \text{ J}$.

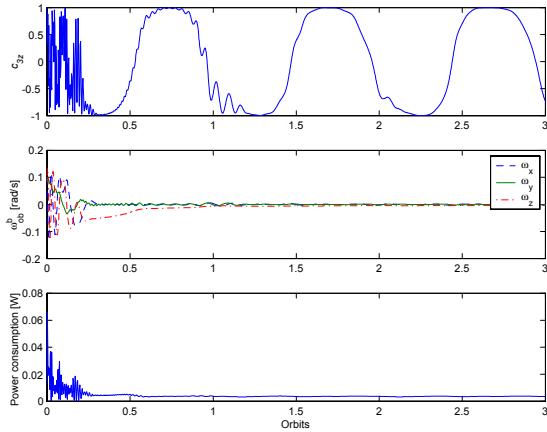


Figure 7: Detumble mode simulation

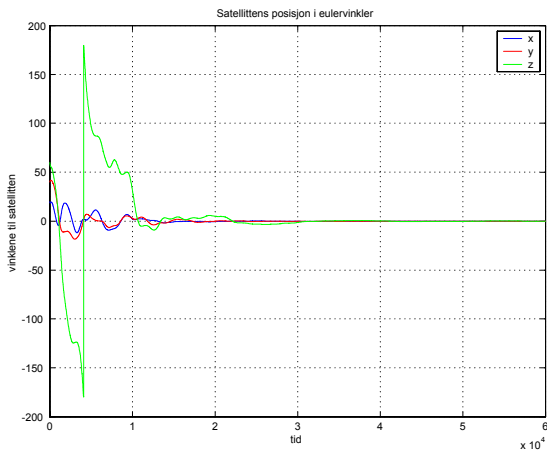


Figure 8: The stabilized attitude of nCube

6.2 Stabilization mode

In Figure 8, the Euler angles of the satellite using the stabilizing controller (23) is shown. A disturbance (white noise) with an amplitude of $\pm 10^{-5}$ T has been added to the magnetometer measurements, and as can be seen the satellite is stabilized. The corresponding magnetic moments from the coils are shown in Figure 9, and as can be seen they are within the specifications. The total energy V of the satellite as well as the angular velocity is shown in Figure 10.

6.3 Inverted boom recovery mode

The inverted boom mode controller (26) was simulated with initial values: $\omega_{ob}^b = (0.0005 \ 0.0005 \ -0.0003)^T$ rad/s and roll, pitch and yaw angles of 160° , 10° and 20° respectively, and controller parameters: $k_{br} = -900$. In Figure 11 a simulation of the inverted boom procedure is shown.

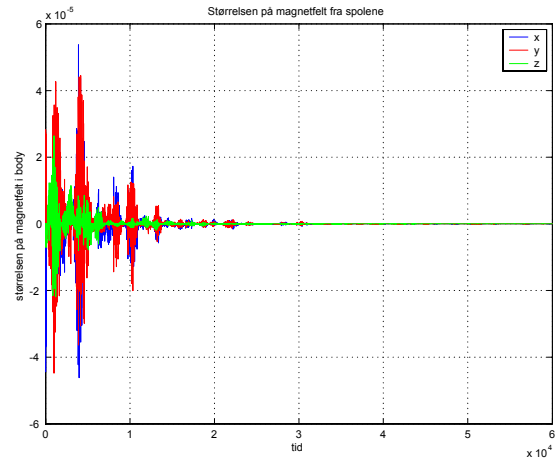


Figure 9: The magnetic moment from the three coils

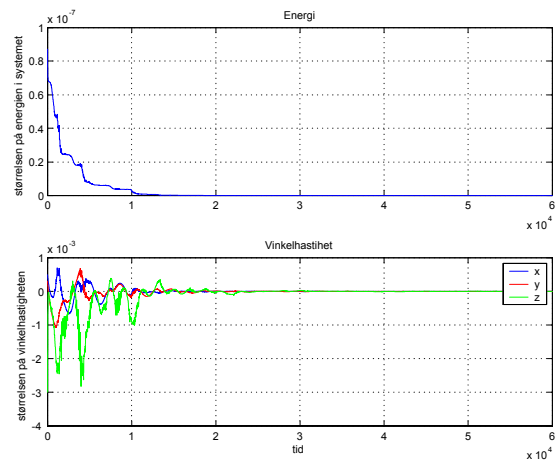


Figure 10: Energy and angular velocity

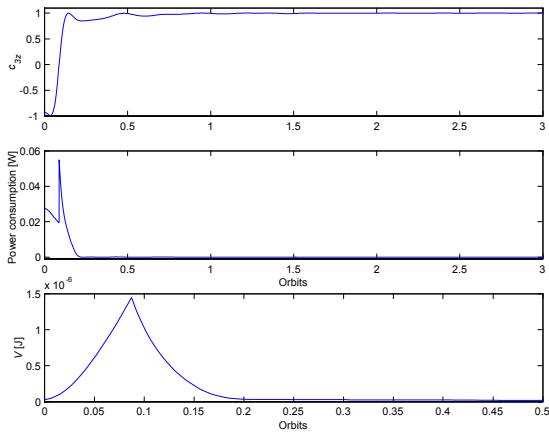


Figure 11: Simulation of the inverted boom controller. In the lower plot the total energy for the first half orbit is shown.

Initially the boom points away from Earth. Average power consumption is $\bar{P} = 1.4$ mW, while the total energy used for three orbits is $E = 24.1$ J. The satellite is turned around very quickly. The lower plot shows the total energy of the satellite. Initially the destabilizing controller increases the energy of the system, until the boom crosses the horizontal plane. Then the stabilization controller is activated and the energy is dissipated.

7 Further work

Ongoing work in this project includes final design of the determination system and implementation of the complete ADCS on microcontrollers. The final satellite will undergo assembly and testing during spring 2004 and launch is planned for autumn 2004.

8 Acknowledgements

The authors gratefully acknowledges the support of The Norwegian Space Center, ESA, Andøya Rocketrange and the Department of Engineering Cybernetics, NTNU

References

- [1] "Http://Www.Rocketrange.No/Ncube/," Web site of the Ncube project, September, 2003.
- [2] Riise, Å.-R., Samuelsen, B., Sokolova, N., Cederblad, H., Fasseland, J., Nordin, C., Otterstad, J., Fauske, K., Eriksen, O., Indergaard, F., Svartveit, K., Furebotten, P., Sæther, E., and Eide, E., "Ncube: The First Norwegian Student Satellite," In *Proceedings of The 17th AIAA/USU Conference on Small Satellites*, 2003.

- [3] Egeland, O. and Gravdahl, J., *Modeling and Simulation for Automatic Control*, Marine Cybernetics, Trondheim, Norway, 2002.
- [4] Wertz, J., *Space Mission Analysis and Design*, Kluwer academic publishers, London, 3rd ed., 1999.
- [5] Kristiansen, R., *Attitude Control of Mini Satellite*, Master's thesis, NTNU, 2000.
- [6] Egeland, O., "Norwegian Ionospheric Small Satellite Experiment Attitude Control and Determination System," Tech. Rep. 94-72-W, Sintef, 1994.
- [7] Indergaard, F., *Design and Implementation of a Gravity Boom for the Norwegian Nano Satellite Ncube*, Master's thesis, NTNU, 2003.
- [8] Busterud, B., *Oreinteringsregulering Av Mikrosatellitter*, Master's thesis, NTNU, 2003.
- [9] Hughes, P., *Spacecraft Attitude Dynamics*, Wiley, New York, 1986.
- [10] Soglo, P., *3-Aksestyring Av Gravitasjonsstabilisert Satelitt Ved Bruk Av Magnetspoler*, Master's thesis, NTNU, 1994.
- [11] Wisniewski, R., *Satellite Attitude Control Using Only Elecromagnetic Actuation*, Ph.D. thesis, Dept. of Control Engineering, Aalborg University, Denmark, 1996.
- [12] Vidyasagar, M., *Nonlinear Systems Analysis*, Prentice-Hall, Englewood Cliffs, NJ, 1993.
- [13] Matrosov, V., "On the Stability of Motion," *J. Appl. Math. Mech*, Vol. 26, 1962, pp. 1337–1353.
- [14] Loria, A., Panteley, E., Popovic, D., and Teel, A., "An Extension of Matrosov's Theorem with Application to Stabilization of Nonholonomic Control Systems," *Proceedings of the 41st IEEE Conference on Decision and Control*, Las Vegas, NV, 2002, pp. 1528–1533.
- [15] Svartveit, K., *Attitude Determination of the Ncube Satellite*, Master's thesis, NTNU, 2003.
- [16] Appel, P., "Attitude Estimation from Magnetometer and Earth-Albedo-Corrected Coarse Sun Sensor Measurements," *Proceedings of the 4th International Symposiums on Small Satellites for Earth Observation*, Berlin, 2003.
- [17] Brown, R. and Hwang, P., *Introduction to Random Signals and Applied Kalman Filtering*, Wiley, 1997.
- [18] Psiaki, M., Martel, F., and Pal, P., "Three-Axis Attitude Determination Via Kalman Filtering of Magnetometer Data," *J. of Guidance, Control and Dynamics*, Vol. 13, No. 3, 1990, pp. 506–514.
- [19] Bak, T., *Spacecraft Magnetometer Determination - A Magnetometer Approach*, Ph.D. thesis, Dept. of Control Engineering, Aalborg University, Denmark, 1999.